11-2021

Effects of Material Texture and Packing Density on the Interfacial Polarization of Granular Soils

Hang Chen
Boise State University

Qifei Niu
Boise State University

Effects of Material Texture and Packing Density on the Interfacial Polarization of Granular Soils

Hang Chen
Boise State University

Qifei Niu*
Boise State University
qifeiniu@boisestate.edu

Abstract

Many electrical and electromagnetic (EM) methods operate at MHz frequencies, at which the interfacial polarization occurring at the solid-liquid interface in geological materials may dominate the electrical signals. To correctly interpret electrical/EM measurements, it is therefore critical to understand how the interfacial polarization influences the effective electrical conductivity and permittivity spectra of geological materials. In this study, we employ pore-scale simulation to study the role of material texture and packing in the interfacial polarization in water-saturated granular soils. Synthetic samples with varying material textures and packing densities are prepared with the discrete element method. The effective electrical conductivity and permittivity spectra of these samples are determined by numerically solving the Laplace equation in a representative elementary volume of the samples. The numerical results show that the effective permittivity of granular soils increases as the frequency decreases due to the polarizability enhancement from the interfacial polarization. The induced permittivity increment is mainly influenced by the packing state of the samples, increasing with the packing density. Material textures such as the grain shape and size distribution may also affect the permittivity increment, but their effects are less significant. The frequency characterizing the interfacial polarization (i.e., characteristic frequency) is mainly related to the electrical contrast of the solid and water phases. The model based on the traditional differential effective medium (DEM) theory significantly underestimates the permittivity increment by a factor of more than two and overestimates the characteristic frequency by ~ 1MHz. These inaccurate predictions are due to the fact that the electrical interactions between neighboring grains are not considered in the DEM theory. A simple empirical equation is suggested to scale up the theoretical depolarization factor of grains entering the DEM theory to account for the interaction of neighboring grains in granular soils.

Introduction

Electrical and electromagnetic (EM) tools have been proven to be useful in imaging the structure and processes of both deep and shallow subsurface (e.g., Nobes, 1996; Weiss and Constable, 2006; Munoz, 2014). Commonly-used electrical and EM methods include the traditional electrical resistivity method (Samouëlian et al., 2005), complex resistivity method (e.g., Wu et al., 2013), EM induction method (West and Macnae, 1991), magnetotellurics (Simpson and Bahr, 2005), capacitive resistivity method (Kuras et al., 2006), time-domain and spectral induced polarization (Binley and Slater, 2020), and ground penetrating radar (GPR) (Annan, 2005). The physical properties measured in electrical and EM surveys are the electrical conductivity (or resistivity) and/or permittivity of the subsurface at the instrument's operating frequency (frequencies). For instance, the traditional electrical resistivity method utilizes direct current (DC), and thus the measured resistivity is the DC resistivity of the subsurface. In contrast, the complex resistivity method and capacitive resistivity methods use an alternating current (AC) with a frequency ranging from ~0.1 Hz to ~ 10^3 Hz (e.g., Kemna et al., 2000; Kuras et al., 2006) and thus, the measured resistivity is the low-frequency resistivity, which may be different from the DC resistivity (e.g., Hauck and Kneisel, 2006). Similarly, the permittivity measured by geophysical instruments operating at different frequencies can be distinct if the dominating polarization mechanism is different (Chelidze and Gueguen, 1999). For spectral induced polarization, which works in the frequency range of 10^{-3} Hz to 10^2 Hz, the measured relative permittivity (normalized by vacuum permittivity) is from ~10^6 to ~10^9 (e.g., Lesmes and Morgan, 2001) and it is mainly associated with low-frequency electrochemical

polarizations (Marshall and Madden, 1959; Revil, 2012). In GPR surveys, the frequency of the EM waves is between 10^6 Hz and 10^9 Hz (Annan, 2005) and thus, the measured relative permittivity (usually < ~79) is the high-frequency permittivity (or dielectric permittivity) arising mainly from the dipolar polarization of water molecules (Lesmes and Friedman, 2005). To correctly interpret electrical and EM measurements, it is necessary to have a mechanistic understanding of the frequency-dependent, effective electrical conductivity and permittivity of geological materials.

At low frequencies (fro m 1 mHz to ~10 kHz), the primary mechanisms controlling the effective electrical conductivity of porous geological materials are the ionic conduction of pore water and the surface conduction arising from the electrical double layer (EDL) formed at the water-mineral interface (Revil and Glover, 1998; Feng et al., 2020). Major factors influencing the low-frequency conductivity of geological materials include the water content, pore water salinity, grain shape and size, packing, and the surface properties of the mineral (Friedman, 2005; Binley and Slater, 2020). The effective permittivity (or imaginary conductivity) of geological materials in this frequency range is predominately controlled by the electrochemical properties of the EDL (Revil, 2012), and material texture and microstructure may also play an important role (Slater and Glaser, 2003).

For frequencies larger than 10^9 Hz, the primary mechanism for the effective permittivity of geological materials is the dipolar polarization of water, and thus water content is the controlling factor influencing the high-frequency permittivity of geological materials. Other factors, such as material texture, microstructure, and fluid chemistry, may also have a non-negligible influence (Martinez and Barnes, 2001). The high-frequency electrical conductivity is, in principle, higher than the DC conductivity due to the influence of various polarizations (e.g., see Niu et al., 2020). However, in practice, the difference between them is usually ignored partly due to the difficulty in measuring geological materials' high-frequency conductivity (Robinson et al., 2003). It is worth noting that most existing electrical conductivity/permittivity models for geological materials were developed for these high- and low-frequency limits. Examples include the well-known Archie's law (Archie, 1942) for DC resistivity and Topp's equation (Topp et al., 1980) for dielectric permittivity.

At intermediate frequencies (from ~10 kHz to ~100 MHz), it is well accepted that the interfacial polarization, which occurs at the interface separating two regions with contrasting electrical properties, will influence the effective conductivity and permittivity of heterogeneous materials (e.g., Hanai, 1960). At the microscopic scale, the interfacial polarization can induce an electric dipole moment at the solid-liquid interface of the geological material, in which additional energy is stored from the external electric field. Thus, at the macroscopic scale, the material's polarizability is enhanced, and the effective permittivity becomes larger compared to that at a higher frequency. As a result, the effective conductivity of the material decreases during this process according to the principles of causality (e.g., Milton et al., 1997). By assuming a simplified microstructure, many theoretical models have been developed to describe the effective conductivity and permittivity of porous media or colloidal systems where the influence of interfacial polarization is significant (Hanai, 1960; Chen and Or, 2006; Tabbagh et al., 2009).

The differential effective medium (DEM) theory (Sheng, 1990) has been frequently used to model the variation of electrical properties of geological sediments resulting from the interfacial polarization. In the DEM theory, it is usually assumed that the geological sediment is formed by successively adding grains into a host medium (i.e., water) to reach the target concentration (Sheng and Callegari, 1984). Different grain shapes and orientations can be handled in the modeling (Mendelson and Cohen, 1982), and thus the DEM-based models can, to a certain extent, account for the textural influence on the electrical conductivity and permittivity spectra of granular materials. Early studies (Sen et al., 1981) have shown that the DEM theory can reproduce the empirical Archie's law. It is worth noting that the DEM theory utilized the multiple scattering technique and single-site (or one-site) approximation (Sen et al., 1981). The latter assumes the statistical independence of grains (Sen et al., 1981). That said, neighboring grains are ignored and only the homogenous equivalent medium is considered (p474, Kocks et al., 2000). This is the reason that Sen et al., (1981) commented on their DEM model "*There are two obvious aspects that we have neglected here that contribute to these high values of ε'...First, consider textural features. The effect of grain contact was neglected…*" This single-site approximation could be valid for colloidal suspensions where the volume concentration of solid grains is low , and newly-added grains keep a considerable distance (relative to grain radius) from the existing grains. However, typical geological materials such as soils and sedimentary rocks have a very high concentration of the solid phase (>50% by volume), and the assumption of dilute conditions may not be valid. Thus, it is unclear if the DEM theory can accurately describe the electrical conductivity and permittivity spectra of geological materials with different textures and packing states. Note that it is critical to accurately model the interfacial polarization from both practical and theoretical considerations. In practice, many geophysical tools work in the frequency range from 1 kHz to 10 MHz

where interfacial polarization is significant. An accurate model of the interfacial polarization-induced permittivity variation will help better interpret many geophysical measurements. From a theoretical point of view, analyzing the possible limitations of the DEM theory will help us better understand the effective properties of geological materials that have complex microstructures and textures.

It is challenging to experimentall y study the effects of material texture and packing density on the interfacial polarization in geological materials for the following reasons. First, it is difficult and costly to characterize the material's texture and microstructure, for example, with advanced pore-scale imaging techniques (e.g., Blunt et al., 2013). Second, most geological minerals are surface-charged due to isomorphous substitutions (McBride, 1989) or the presence of hydroxyl groups (Zhuravlev, 2000), and thus EDLs can form at the charged surface when the material is in contact with water. Under an external field, the EDL could disturb the local ion transport and electric field, thus altering the material's effective conductivity and permittivity (Revil and Glover, 1998; Revil, 2012; Bücker and Hördt, 2013). In general, the influence of the EDL on the effective electrical properties of geological materials outweighs the interfacial polarization, and thus it is difficult to discern the effect of interfacial polarization from the measured electrical responses.

In the last decade, the pore-scale numerical simulation (e.g., Dvorkin et al., 2011; Andrä et al., 2013) has emerged as a powerful tool for studying the electrical properties of geological materials, such as DC resistivity (e.g., Zhan et al., 2010) and dielectric permittivity (e.g., Han and Yang, 2018). Recently, the low-frequency electrochemical polarizations have been considered (e.g., Niu and Zhang, 2017), and thus it is possible to model the broadband electrical conductivity and permittivity of geological materials (Niu et al., 2020). In such pore-scale simulations, the effective conductivity/permittivity of a sample is calculated by directly solving the Laplace equation in a representative elementary volume (REV) of the sample, and the material's texture and microstructure can be easily characterized (Andrä et al., 2013), providing a powerful tool for studying the textural and microstructural effects on effective properties of heterogeneous geological materials.

Here, we employ pore-scale numerical simulation to study the interfacial polarization in water-saturated granular soils. The focus is on the effect of material texture and packing on the electrical conductivity and permittivity spectra. In our simulations, the surface conduction (Revil and Glover 1998) is not included because its effect on interfacial polarization could complicate the interpretation of the material packing/texture effect. However, it can be easily added in further studies to form a complete understanding of interfacial polarization in geological materials. The water conductivity considered in this study is between 0.001 S m^{-1} and 0.1 S m^{-1}, which are typical for groundwater. Considering these assumptions, the results presented here may not be directly used in petroleum engineering but have implications for groundwater exploration where surface conduction is low. An example is hydrogeophysical studies that involve coarse sediments such as unconsolidated acquirer characterization.

This paper is organized as follows. The theoretical background of interfacial polarization, including the mechanism and theoretical modeling, will be briefly reviewed first. We then describe the details of the pore-scale numerical simulation and the preparation of synthetic samples. The numerical results are presented afterward and compared with the predictions from the DEM theory. We also suggest an updated DEM model that corrects the influence of neighboring grains on the depolarization factor of individual grains to better describe the permittivity of granular soils. Major conclusions are summarized at the end of the paper.

Theoretical Background

Frequency-Dependent Permittivity

The permittivity quantifies a material's ability to store energy from an external electric field. For water-saturated geological materials, the effective permittivity generally increases as the frequency decreases, as shown in Figure 1a. This is because, as the frequency of the external electric field decreases, polarizations with a longer characteristic time (or larger length scale) are triggered, enhancing the existing polarizations with shorter characteristic times (or smaller length scales). The macroscopic response of the material is that the measured effective permittivity increases, as shown in Figure 1 (also see Niu et al., 2020). As the permittivity increases, more energy is stored in the material from the external electric field. As a result, less conductive current passes through the material, and the electrical conductivity of the material decreases as the frequency decreases (Niu et al., 2020). In geological materials, typical polarization mechanisms include dipolar polarization of water molecules, interfacial polarization, and electrochemical polarization (Figure 1).

Interfacial Polarization Mec hanism

Considering a heterogeneous material with a spatial distribution of the electrical conductivity σ and permittivity ε, we have the following equations,

$$\nabla \cdot \mathbf{D} = \rho, \tag{1}$$

$$\mathbf{J} = \sigma \mathbf{E}, \tag{2}$$

and

$$\mathbf{D} = \varepsilon \mathbf{E}, \tag{3}$$

where **D** is the displacement field, ρ is the net charge density (C m^{-3}), **J** is the conductive current density, and **E** is the electric field. Also, the continuity equation is

$$\nabla \cdot \mathbf{J} = \frac{\partial \rho}{\partial t} \tag{4}$$

where t is time. Considering a sinusoidal change of ρ with t, inserting equation 2 into equation 3 yields

$$j\omega\rho = \nabla\sigma \cdot \mathbf{E} + \sigma \nabla \cdot \mathbf{E}. \tag{5}$$

Similarly, inserting equation 3 into equation 1 yields

$$\rho = \nabla\varepsilon \cdot \mathbf{E} + \varepsilon \nabla \cdot \mathbf{E}. \tag{6}$$

Equation 6 is used to cancel the term $\nabla \cdot \mathbf{E}$ in equation 5 and then we have

$$j\omega\rho = \frac{\sigma}{\varepsilon}\rho - \frac{\sigma^2}{\varepsilon}\left(\nabla \frac{\varepsilon}{\sigma} \cdot \mathbf{E}\right). \tag{7}$$

Approaching the DC limit of equation 7 results in the following equation (Alvarez, 1973),

$$\rho = \sigma \left(\nabla \frac{\varepsilon}{\sigma} \cdot \mathbf{E}\right). \tag{8}$$

Equation 8 states that, in heterogeneous materials, a net charge will form in regions where ε/σ is inhomogeneous (Alvarez, 1973). Consider a grain-water mixture shown in Figure 2a. Assume ε and σ in each phase are homogenous, but the ratio ε/σ is different for the grain and water. It is also assumed that no surface charges are present. At the solid-water interface (Figure 2b), the electric potential u and total current density $\varepsilon^* \frac{du}{dx}$ are continuous, but the electric field $\frac{du}{dx}$ and the electrical property (i.e., ε/σ) are discontinuous. Here, ε^* is the complex permittivity, expressed as $\varepsilon + j\sigma/\omega$ where j is the imaginary unit, ω is the angular frequency, and x is the distance from the interface in the normal direction (Figure 2c). Since the ratio ε/σ has a sharp change at the solid-water interface [i.e., $\nabla(\varepsilon/\sigma)$ is non-zero], according to equation 8, a net charge will form in this region. On the other side of the interface, the sign of $\nabla(\varepsilon/\sigma)$ is reversed, and thus the net charge density ρ is opposite (Figure 2c). This means the positive and negative charges are separated by the solid-water interface (Figure 2a), and thus the interface of the material is polarized. Macroscopically, the effective permittivity of the material increases if compared to that at a higher frequency (e.g., Figure 1). This phenomenon is known as the interfacial polarization or Maxwell-Wagner polarization (e.g., Chen and Or, 2006).

Wagner Equation

In the past, many theoretical models have been developed to model the interfacial polarization-induced variations of the effective electrical properties of heterogeneous materials. One of the earliest models is the Wagner equation (Wagner, 1914) for composites consisting of spherical grains (phase 2) *sparsely* distributed throughout a host medium (phase 1). The effective complex permittivity ε^*_{eff} of the composite is expressed as (e.g., Choy, 2015)

$$\frac{\varepsilon^*_{eff} - \varepsilon^*_1}{\varepsilon^*_{eff} + 2\varepsilon^*_1} = f_2 \frac{\varepsilon^*_2 - \varepsilon^*_1}{\varepsilon^*_2 + 2\varepsilon^*_1} \tag{9}$$

where f_2 is the volume fraction of phase 2, ε^*_1 and ε^*_2 are the complex permittivity of phase 1 and phase 2, respectively. The complex permittivity ε^*_{eff}, ε^*_1, and ε^*_2 can be linked to their corresponding conductivity σ_i and permittivity ε_i by $\varepsilon^*_i = \varepsilon_i + j\sigma_i/\omega$ where i = *eff*, 1, or 2. Note that equation 9 assumes that the inclusion concentration is low (i.e., the dilute assumption), implying no electric interaction between neighboring grains.

Differential Effective Medium (DEM) Theory

In the DEM theory (e.g., Hanai, 1960; Sen et al., 1981; Sheng and Callegari, 1984), a composite is constructed by starting from a homogeneous medium with the following iterative processes: (1) replace a small amount of this homogeneous component by the second component, (2) treat the resulting mixture as a homogeneous component, and (3) repeat steps 1 and 2 until the concentration of the second component reaches the target value. This iterative process can be described by a differential equation (e.g., Mendelson and Cohen, 1982). With properly defined boundary conditions and homogenization method (i.e., how the two components are averaged), the resulting differential equation can be solved to link the heterogeneous material's effective properties to the properties of its constitutes. In DEM modeling, the shape and orientation of the infinitesimal element replaced by the second component can be specified, and thus, the material texture can be accounted for. Existing DEM theory-based models usually use ellipsoidal inclusions, and their shape and orientation follow predefined distributions (e.g., Mendelson and Cohen, 1982). Although the DEM theory was originally proposed for two-phase mixtures, it has also been extended to three-phase mixtures (e.g., Norris et al., 1985; Chen and Or, 2006).

Now we consider a water-saturated granular material and apply the DEM theory to replace the host medium (water) with spherical grains. If the homogenization process after each replacement is described by the Wagner equation (equation 9), the effective complex permittivity ε^*_{eff} of the granular material can be derived analytically as (Hanai 1962)

$$\phi = \frac{\varepsilon^*_{eff} - \varepsilon^*_s}{\varepsilon^*_w - \varepsilon^*_s}\left(\frac{\varepsilon^*_w}{\varepsilon^*_{eff}}\right)^{1/3} \tag{10}$$

where ε^*_s and ε^*_w are the complex permittivity of the grain and water, respectively, and ϕ is the material's porosity. Note that the complex permittivity ε^*_w (or ε^*_s) can be linked to water (or solid phase) conductivity σ_w (or σ_s) and permittivity ε_w (or ε_s) by $\varepsilon^*_w = \varepsilon_w + j\sigma_w/\omega$ (or $\varepsilon^*_s = \varepsilon_s + j\sigma_s/\omega$). If the shape of the replaced infinitesimal element is a spheroid (ellipsoid of revolution), a water-saturated granular material made of spheroidal grains can now be modeled. If the orientation of the grains is further assumed to be random, the effective complex permittivity ε^*_{eff} of the material can be derived analytically as (e.g., Lesmes and Friedman, 2005)

$$\varepsilon^*_{eff} = \varepsilon^*_w \phi^m \left(\frac{1-\varepsilon^*_s/\varepsilon^*_w}{1-\varepsilon^*_s/\varepsilon^*_{eff}}\right)^m \tag{11}$$

and the porosity exponent m is defined by (Mendelson and Cohen, 1982)

$$m = \left\langle \frac{5-3L}{3(1-L^2)} \right\rangle \tag{12}$$

where L is the depolarization factor along the principal axis of spheroidal grains with the smallest length and the bracket $\langle\ \rangle$ indicates an average over all L values if the grains have a distribution of shapes. Define a_x, a_y, and a_z as the semi-axes of an ellipsoid in the three orthogonal directions, and the depolarization factor of the ellipsoid in the x-direction L_x can be theoretically calculated from (e.g., Sihvola and Kong, 1988)

$$L_x = \frac{a_x a_y a_z}{2}\int_0^\infty \frac{ds}{(s+a_x^2)\sqrt{(s+a_x^2)(s+a_y^2)(s+a_z^2)}}. \tag{13}$$

The depolarization factor in other directions L_y (or L_z) can also be calculated from equation 13 by interchanging a_x and a_y (or a_x and a_z) in the above integrand. Note that L_x, L_y, and L_z are related to each other by

$$L_x + L_x + L_x = 1. \tag{14}$$

For spheres, $L_x = L_y = L_z = 1/3$, and thus equation 11 reduces to equation 10.

Samples and Simulations

In this study, we adopt the method used in Niu and Zhang (2018) to generate six synthetic granular samples featuring different material textures (grain shape and size) and packing densities. The broadband, effective electrical properties of these samples are numerically determined using pore-scale simulations (e.g., Niu et al., 2020). In this section, the details of the synthetic sample generation and pore-scale simulation are presented.

Synthetic Soil Samples

In this study, the synthetic soil samples are generated using the discrete element method (Cundall and Strack, 1979), which is a numerical scheme capable of describing the mechanical behavior of assemblies of grains with various shapes. In the simulation, the mechanical interaction between touching grains is described by local contact laws such as the Hertz-Mindlin model (e.g., Radjaï and Dubois, 2011). Under external stress/strain conditions, contacts between grains are updated continuously to reach equilibrium. During this process, existing contacts may be lost, and new contacts may be established. Based on the displacement and rotation of each grain, the macroscopic mechanical properties of the sample can be determined. The discrete element method has been widely used in the geomechanical community to gain microscopic insights into the stress-strain behavior of geological materials (e.g., Cheng et al., 2004; Zhao and Guo, 2013).

In this study, the open-source DEM software OVAL developed by Kuhn (2006) (available at http://faculty.up.edu/kuhn/oval/oval.html) is used to generate the granular samples. In total, six samples made of spheroidal grains were prepared, and they are the same samples used in Niu and Zhang (2018). For each of the samples, all the grains have the same shape with e = 1, 0.5, or 0.67 where e is the ratio of the semi-minor b to semi-major axes a. Although a normal or lognormal distribution of grain size is more representative of real soils, it is computationally challenging to include grains with a broad size range in a pore-scale simulation. For simplicity, in this study the grain size a is either a constant or following a uniform distribution in the range [0.5a, 1.5a]. In preparing each sample, 8000 grains are generated with their initial positions and orientations randomly distributed in a cube. The boundary walls enclosing the cube then move slowly inward to compress the sparse granular assembly until it reaches a very loose state, i.e., the confining pressure reaches ~1 kPa. A denser packing state of the sample can be achieved by further compressing the loose assembly. A dilute state of the sample can be obtained by simultaneously reducing the size of all the grains of the loose assembly (Niu and Zhang, 2018). With these procedures, realistic granular samples with varying material textures and packing densities can be generated. Figure 3 shows the loose packing state of the six synthetic granular soils used in this study.

Pore-Scale Numerical Simulation of Effective Electrical Properties

In laboratory experiments, the effective complex electrical conductivity σ^*_{eff} of a heterogeneous material (e.g., soil) is obtained by applying a known electric field across the sample and measuring the induced current density within the sample (e.g., Friedman 2005). From a microscopic perspective, the applied electric field and induced current density can be treated as the volume-average electric field <**E**> and current density <**J**> of the sample (Torquato, 2013), and thus the effective complex conductivity of the material can be expressed as

$$\sigma^*_{eff} = \frac{\langle \mathbf{J} \rangle}{\langle \mathbf{E} \rangle}. \tag{15}$$

The effective complex permittivity ε^*_{eff} can then be calculated from the complex conductivity as

$$\varepsilon^*_{eff} = j\sigma^*_{eff}/\omega \tag{16}$$

In pore-scale numerical simulations, we solve the Laplace equation to determine the **E** and **J** field in a REV of heterogeneous materials, expressed as

$$\nabla \cdot \mathbf{J} = -\nabla \cdot [\sigma^* \nabla u] = 0 \tag{17}$$

where $\sigma^* = \sigma + j\varepsilon\omega$ is the spatial distribution of complex conductivity in the material. In this study, equation 17 is solved numerically with the finite difference method to determine the spatial distribution of u in the REV of the sample, and an open source code (AC3D.F) developed at the National Institute of Standards and Technology (Garboczi, 1998) is used to conduct the simulation. This software has been widely to calculate the effective electrical properties of various composites (e.g., Torrents et al., 2000; Kidner et al., 2002; Niu and Zhang, 2017). In the calculation, the

periodic boundary condition is maintained. Once the u field is determined, the related **E** and **J** fields can then be calculated. The average electric field <**E**> and current density <**J**> of the REV are calculated as the volume-averaged **E** and **J**. Lastly, the effective complex conductivity σ_{eff}^* and permittivity ε_{eff}^* of the sample are determined by applying equations 15 and 16.

Benchmarking of the Numerical Code

The permittivity change induced by interfacial polarization is relatively small if compared to the intrinsic permittivity of the material at high frequencies (e.g., GHz). In order to analyze the influences of texture and packing using pore-scale simulations, we here perform benchmarking for the numerical code using a spherical grain immersed in water. The cubic domain to be simulated has a length of 20 mm and the centered grain has a radius of 4 mm. Thus, the porosity of the grain-water mixture is 96%. For this simple grain-water system, both the Wagner equation (equation 9) and DEM theory (equation 10) are exact in describing the effective permittivity (e.g., Torquato, 2013).

The cubic domain of the grain-water mixture is discretized into a number of voxels with equal size d, and each voxel is assumed homogeneous (Garboczi, 1998). If the voxel is in the water phase, it has the same electrical properties as the water phase; otherwise, the electrical properties of the solid phase will be assigned. In the simulation, the water conductivity σ_ω is 0.01 S m$^{-1,}$ and the permittivity of water is $80\varepsilon_0$ where ε_0 is the vacuum permittivity; the solid phase is an insulator (i.e., $\sigma_s = 0$ S m^{-1}) and has a permittivity of $5\varepsilon_0$. The complex conductivity of the water and solid phases are $\sigma_\omega^* = \sigma_\omega + j\omega 80\varepsilon_0$ and $\sigma_s^* = 0 + j\omega 5\varepsilon_0$, respectively.

In the benchmarking, we first used a relatively dense discretization with a total number of discretized voxels $N^3 = 400^3$ where N is the number of discretized intervals in one side of the domain. This means the grain is discretized into ~100^3 voxels. The calculated permittivity of the grain-water mixture for frequencies ranging from 10^3 Hz to 10^9 Hz is presented in Figure 4a. The theoretical values calculated using equation 10 are also shown in the figure (solid line). As shown in the Figure, the numerical and theoretical results agree perfectly. The relative error of the permittivity in this broad frequency range is below 0.001%. This perfect match proves that, with a dense discretization, the numerical simulation code produces an accurate permittivity spectrum.

Although numerical simulations with a dense discretization can ensure accurate permittivity results (Figure 4a), the associated computational cost is high. For granular soils, a REV usually contains several hundred grains. If the same discretization scheme (e.g., ~160^3 voxels for one grain) is used, the calculation of the REV will not be practical for our study. Thus, in our simulation of granular soils, a relatively coarse discretization scheme has to be used. Studies have shown that the discretization scheme could affect the calculated effective properties (e.g., Zhan et al., 2010). To quantify this influence, we conducted a series of simulations on the same domain with different numbers of discretized voxels, $N^3 = 50^3$, 100^3, 200^3, 300^3, and 400^3. These correspond to the grain being discretized into $M^3 = 20^3$, 40^3, 80^3, 120^3, and 160^3.

To quantitatively estimate the error induced by a coarse discretization, we define two parameters to describe the influence of interfacial polarization on the permittivity spectra: (1) permittivity increment $\Delta\varepsilon_{eff}$ and (2) characteristic frequency f_c. As shown in Figure 5, the permittivity increment $\Delta\varepsilon_{eff}$ is defined as the permittivity difference between the low- and high-frequency limits; the characteristic frequency f_c is the frequency at which the permittivity is equal to the average permittivity of the low- and high-frequency limits. Since the simulated permittivity is discrete in the frequency domain, a second-order polynomial curve is used to fit the numerical data to determine f_c. Other frequencies may also be used to characterize the interfacial polarization such as the frequency at which the derivative of the permittivity reaches its maximum value.

The influence of discretization on $\Delta\varepsilon_{eff}$ and f_c of the aforementioned grain-water mixture is shown in Figure 6. It is clear that a coarse discretization introduces numerical errors to both $\Delta\varepsilon_{eff}$ and f_c. If the grain is discretized into ~40^3 instead of ~160^3 voxels, the relative error of $\Delta\varepsilon_{eff}$ increases from less than 1% to ~17%. Comparing to $\Delta\varepsilon_{eff}$, the influence of discretization on f_c is minimal. In this study, we take a cubic REV with a length of 3 mm from each granular sample. As a trade-off between computational cost and numerical accuracy, the REV is discretized into 300^3. With this discretization scheme, each grain in the granular soil is discretized into ~40^3 voxels. According to Figure 6, the relative error is expected to be ~17% for the calculated $\Delta\varepsilon_{eff}$ and ~ 2% for f_c.

Simulation Results and Comparison with DEM Theory

General Trend

The calculated effective electrical conductivity σ_{eff} and permittivity ε_{eff} spectra of the uni-sized sample with spheres assembly are presented in Figure 7. It is shown that both σ_{eff} and ε_{eff} of the sample experienced a noticeable change around 1 MHz. In general, as the frequency decreases, ε_{eff} increases, indicating enhanced polarizability of the sample. Accordingly, σ_{eff} decreases as the frequency decreases. For example, the relative permittivity of the sample at $\phi = 30\%$ (Figure 7b) increases from ~16 at 100 MHz to ~20 at 100 kHz and the effective conductivity (Figure 7a) decreases from ~1.44 to ~1.31 mS m^{-1}. These observed variations in the conductivity and permittivity spectra are caused by the interfacial polarization occurring at the solid-water interfaces of the granular soils.

Effect of Packing Density

In Figure 7, it is apparent that the packing density (or porosity) of the sample has a dominating effect on the effective electrical properties. In general, as the packing density increases (i.e., ϕ decreases), the manifestation of interfacial polarization is more obvious. The permittivity incremental $\Delta\varepsilon_{eff}$ and characteristic frequency f_c of the samples with $e = 1$ are determined for all the packing densities, and the results are plotted in Figure 8. Both uni-sized and multi-sized samples are included. It is shown in Figure 8 that $\Delta\varepsilon_{eff}$ continuously increases as the porosity of the sample decreases, increasing from ~$0.06\varepsilon_0$ at $\phi = 89\%$ to ~$2.5\varepsilon_0$ at $\phi = 30\%$. The relative permittivity increment ($\Delta\varepsilon_{eff}/\varepsilon_L$ where ε_L is the low frequency permittivity, e.g., at 1 kHz) is ~0.1% at $\phi = 89\%$ and ~12.5% at $\phi = 30\%$. At the dilute condition (i.e., ϕ >60%), the increase in $\Delta\varepsilon_{eff}$ with packing density is minimal if compared with that at the concentrated condition (Figure 8a). The characteristic frequency f_c also varies with the porosity or packing density (Figure 8b), decreasing from ~2 MHz at $\phi = 89\%$ to ~1 MHz at $\phi = 30\%$. Similar to $\Delta\varepsilon_{eff}$, the variation of f_c at dilute conditions is less significant than that at concentrated conditions (Figure 8b).

The increase in $\Delta\varepsilon_{eff}$ with packing density of granular material has been shown in some other studies (e.g., Hanai, 1962). The value of our simulations is that the grain shapes are accurately controlled. Therefore, the numerical data produced in this study can be used to evaluate if existing theories can quantify the packing effect and the grain shape effect. Thus, we also calculated the f_c and $\Delta\varepsilon_{eff}$ of the samples at different porosities based on the theoretical permittivity spectra from the DEM theory (equation 11), and the results are shown in Figure 8 as solid lines. Numerical error in permittivity increment related to a coarse discretization are indicated by error bars; for the characteristic frequency, the associated numerical error is smaller than the size of the symbol. The general trends of $\Delta\varepsilon_{eff}$ and f_c are similar for theoretical and numerical results. In particular, the DEM theory accurately reproduces the $\Delta\varepsilon_{eff}$ variations of the sample at dilute conditions ($\phi > 60\%$). However, at the concentrated condition ($\phi < 60\%$), the permittivity discrepancies between the theory and simulation are considerable. It appears that the DEM theory significantly underestimates $\Delta\varepsilon_{eff}$ by a factor of ~2 (Figure 8a). The underestimation of $\Delta\varepsilon_{eff}$ in Figure 8a indicates that applying equation 11 to real geological materials, of which the porosity is usually less than 50%, could induce substantial errors. Similarly, f_c discrepancies between the theory and simulation are also observed, particularly for samples with small porosities (Figure 8b).

The results of samples with different grain shapes ($e = 0.5$ and 0.67) are shown in Figures 9 and 10. Similar trends can also be observed, and our discussion of Figure 8 also holds for the samples in Figures 9 and 10. We attribute the observed discrepancies between the theory and simulation at low porosities to the strong electrical interactions between neighboring grains, which were not considered in the DEM theory. As discussed in Section 2, the DEM theory assumes that the newly-formed mixture after adding the second component is still in the dilute condition. That said, the added second component at each step does not exert any electrical influence on existing grains in the mixture. This assumption, however, can be violated if the porosity of the sample is low. We will provide microscopic proof for this argument in the next section.

Effect of the Grain Size Distribution

Comparisons of uni-sized and multi-sized samples in Figures 8, 9, and 10 show that the grain size distribution has only a small effect on the $\Delta\varepsilon_{eff}$ - ϕ and f_c-ϕ relationships of the samples. In particular, for samples made of grains with $e = 1$ and 0.67, the effect of grain size distribution on the interfacial polarization (e.g., $\Delta\varepsilon_{eff}$ and f_c) is negligible (Figure 8 and 9). This observation in simulation is in agreement with the DEM theory (equation 11), in which the grain size is not a model parameter. For samples made of spheroids with $e = 0.5$ (Figure 10), $\Delta\varepsilon_{eff}$ and f_c of uni-sized and multi-

sized samples are noticeably different for all the studied packing densities. In particular, when the samples are at concentrated conditions ($\phi < 60\%$), the differences are considerable. For example, $\Delta\varepsilon_{eff}$ of the multi-sized sample is generally ~50% higher than that of the uni-sized sample (Figure 10a). In summary, the grain size does have some influence on the interfacial polarization, particularly at concentrated conditions. Compared to the effect of packing density, the grain size effect, however, is less important. It should be noted that, the above conclusion is made for materials with relatively large grains. In real geological materials containing small grains (e.g., nanometers in diameter), other polarizations may overlap with the interfacial polarization and the grain size effect could be more significant.

Effect of Grain Shape

To study the effect of grain shape, we summarize the results of uni-sized samples with three grain shapes in Figure 11. The theoretical curves calculated from the DEM theory (equation 11) are also plotted in the figure. It is shown that, in general, the permittivity increment at a given packing density increases as the grains become more aspherical (e decreases), indicating a strong grain shape effect. For instance, $\Delta\varepsilon_{eff}$ of the sample with $e = 1$ is ~$1\varepsilon_0$ at $\phi = 40\%$ but the value increases to ~$2\varepsilon_0$ for the sample with $e = 0.5$. This is probably because, as the grain becomes aspherical, the total area of the solid-liquid interface within a given sample volume becomes larger, which will enhance the interfacial polarization. Therefore, the induced permittivity increment $\Delta\varepsilon_{eff}$ becomes higher. To support this argument, we calculate the normalized surface area S_v (normalized by the sample volume) for all the samples at different packing densities, and the results are shown in Figure 12. It is apparent that $\Delta\varepsilon_{eff}$ is positively correlated to S_v and other factors such as grain shape and size distribution only have a minor influence on $\Delta\varepsilon_{eff}$.

In contrast, the effect of grain shape on f_c is relatively weak. As shown in Figure 11b, the f_c-ϕ relationships are almost identical for samples with different grain shapes. This observation indicates that material texture may not be the controlling factor of f_c. Indeed, since the interfacial polarization arises from the electrical discontinuity (see equation 8), the electrical contrast (i.e., ε/σ) of the water and grains should have a significant influence on f_c.

Effect of Water Conductivity

To study the effect of water conductivity σ_w, we use the pore-scale simulation to calculate the permittivity spectra of the sample made of uni-sized spheres ($\phi = 45\%$) with different σ_w values. In the simulation, the permittivity of water ($80\varepsilon_0$) and solid phase ($5\varepsilon_0$) are kept unchanged, and five water conductivity values (σ_w = 0.1, 0.0032, 0.01, 0.0316, and 0.001 S m^{-1}) are considered. The permittivity increment $\Delta\varepsilon_{eff}$ and characteristic frequency f_c are determined and shown in Figure 13 along with the theoretical results from the DEM theory (equation 11). It is evident that σ_w has a significant effect on f_c. As σ_w decreases from 0.1 S m^{-1} to 0.001 S m^{-1} (electrical contrast ε/σ increases), the permittivity spectrum shifts towards the low frequencies. The associated f_c varies considerably, decreasing from ~10 MHz to ~100 kHz. Compared to the influence of material texture (grain shape and size) and packing density (Figure 11), the σ_w-induced f_c variation is much more profound. The permittivity increment $\Delta\varepsilon_{eff}$, however, does not change with water conductivity (Figure 13a). In general, the DEM theory gives similar trends for both $\Delta\varepsilon_{eff}$ and f_c as the numerical simulation although there is a small discrepancy. In short, Figure 13 shows that the electrical contrast is the dominating factor affecting the frequency where interfacial polarization occurs.

Electrical Interaction between Neighboring Grains

In the previous section, comparisons of numerical and theoretical results show that the DEM theory-based equation 11 systematically underestimates the permittivity increment and overestimates the characteristic frequency of the interfacial polarization in water-saturated granular soils, especially in concentrated conditions. We argue that these discrepancies are caused by the strong electrical interaction between neighboring grains. In the DEM theory, it is assumed that the addition of new grains into the grain-water mixture does not alter the local electric field near the existing grains (i.e., the dilute assumption). In this section, we provide evidence showing that the dilute assumption will break down when the neighboring grains in granular soils are too close to each.

Depolarization Factor of Two Approaching Grains

As shown in equation 14, the depolarization factor L of a spheroid in a specific direction is theoretically related to its geometry only, and thus its size and distance to a neighboring grain are not accounted for in the DEM theory-based equation 11. However, as a grain approaches a neighboring grain, the local electric field around and within the grain

is altered, affecting its depolarization factor. Here, we use the pore-scale simulation to calculate the depolarization factor of two approaching spheroidal grains (Figure 14a). In the simulation, two grains with the same size (a = 20 μm) and shape (e = 1, 0.67, or 0.5) are considered. The two grains with σ_s = 0 S m^{-1}and $\varepsilon_s = 5\varepsilon_0$ are immersed in water with σ_w = 0.1 S m^{-1}and $\varepsilon_w = 80\varepsilon_0$. The separation between the two grains s is defined as the distance from grain edge to edge (Figure 14a) and varies from zero to ~5a in the simulation. The numerical method proposed in Mejdoubi and Brosseau (2006) and the finite element method software Comsol Multiphysics (COMSOL Inc, Burlington, MA, USA) are used to calculate L. In the calculation, an external electric field is applied to the grain-water mixture in the b direction (Figure 14a). The simulated domain is much larger than the grain volume (ϕ > 85%) so that L can be determined by fitting an analytical mixture theory (e.g., the Maxwell Garnet equation or the symmetric Bruggeman equation) to the calculated effective permittivity of the grain-water mixture. For the details of the numerical simulation, readers can refer to Mejdoubi and Brosseau (2006).

The numerical results are shown in Figu re 14b along with the theoretical L values, which are calculated with a continuous second-order fitting equation proposed by Jones and Friedman (2000), expressed as,

$$L = \frac{1}{1+1.6e+0.4e^2}. \tag{18}$$

In Figure 14b, the simulated L is very close to theoretical values for all the grain shapes when the separation s is larger than ~ 5a. As s decreases, the simulated L continuously increases. When the two grains are in contact with each other, L of the sphere (e = 1), for example, increases by ~ 27% compared to its original value L = 0.33. The increased L in Figure 14 indicates that the existence of a neighboring grain can make the L of a grain deviate from its theoretical value. In granular soils, most neighboring grains have direct contacts, and thus the average separation between neighboring grains is expected to be within several grain radii. As the packing becomes denser, the average grain separation tends to be even smaller. This means, in addition to grain geometry and orientation, the actual L of grains in granular soils should also depend on the distances between neighboring grains and thus the packing density (or porosity) of the sample.

An Updated DEM Model

To correctly model the effective complex permittivity of granular materials, it is necessary to include the influence of neighboring grains on L in the DEM theory. In this study, we suggest a simple power function to correct the theoretical depolarization factor L such that the electrical interaction of neighboring grains can be considered. The power function is expressed as

$$L' = L\phi^p \tag{19}$$

where L' is the actual depolarization factor and p is an exponent smaller than zero. When the grain-water mixtures are at dilute conditions (ϕ > 60%), L' is very close to L; at concentrated conditions (ϕ < 60%), however, L' will deviate considerably from the theoretical L to account for the electrical interaction of neighboring grains. The proposed equation 19 and existing equations 11 and 18 are used to fit the numerical data in Figures 8, 9, and 10, and the results are shown in Figure 15. For samples with e = 1, 0.67, and 0.5, the fitted p values are -0.72, - 0.45, and -0.38, respectively. Compared to Figure 11, the suggested model captures the dominating effect of packing density on both $\Delta\varepsilon_{eff}$ and f_c of samples with different material textures. The associated root-mean-square-deviations (RMSDs) are only 0.21, 0.16 and 0.35 for $\Delta\varepsilon_{eff}$ in Figures 15a, 15b, and 15c, much smaller than the values in Figure 11a (0.71, 0.61 and 1.2). The RMSDs values for f_c in Figure 15 (0.28, 0.24, and 0.27 MHz) are also much smaller than those in Figure 11b (0.45, 0.40, and 0.50 MHz). The good fit in Figure 15 indicates that the suggested model can describe the interfacial polarization-induced permittivity variations of water-saturated granular soils with varying texture and packing states. However, it should be addressed that although equation 19 can provide qualitative trends on the behavior of depolarization factor for grains in close contact, it should not be regarded as a quantitatively predictive model. More data (both numerical and experimental) are required in order to improve the existing DEM models in describing the permittivity variations induced by interfacial polarization in geological materials.

Conclusion

Pore-scale numerical simulations conducted in this study show that the interfacial polarization induces noticeable variations in the effective complex permittivity or conductivity of water-saturated granular soils in the intermediate frequency range (~ 100 kHz to ~100 MHz). The effective permittivity of granular soils increases as the frequency

decreases due to the polarizability enhancement from the interfacial polarization occurring at the solid-water interface. As a result, the effective conductivity of the samples decreases as the frequency decreases. The associated permittivity increment is predominantly controlled by the packing state of the granular soils, increasing with the packing density. Material texture such as the grain shape and size distribution can also affect the permittivity increment. As the grain becomes more aspherical, the manifestation of interfacial polarization is more pronounced. This is due to the fact that samples with aspherical grains have a larger area of solid-liquid interfaces where the interfacial polarization will occur. The simulation results also reveal that the frequency characterizing the interfacial polarization in granular soils is mainly controlled by the electrical contrast of the solid and water phases. Samples with high water conductivity tend to have a higher characteristic frequency.

The comparison between theory and si mulation shows that the existing DEM theory-based electrical model can describe the interfacial polarization-induced permittivity variations of grain-water mixtures only at dilute conditions (i.e., porosity $\phi > 60\%$). When the samples' porosity is smaller than 60%, the electrical interaction between neighboring grains in the granular soils becomes significant, violating the dilute assumption used in traditional DEM theory. As a result, the DEM theory significantly underestimates the interfacial polarization-induced permittivity increment by a factor of more than two and overestimates the associated characteristic frequency by ~1 MHz. To account for the influence of neighboring grains, we suggest a simple empirical equation to scale up the theoretical depolarization factor of grains entering the DEM theory. Applying the model to six synthetic samples shows that the new model can adequately fit the permittivity increment and characteristic frequency of granular soils with varying textures and packing densities. Further studies on the applicability of the new model for real geological materials are suggested.

Reference

Alvarez, R., 1973, Complex dielectric permittivity in rocks: A method for its measurement and analysis: Geophysics, **38**, no. 5, 920-940.

Andrä, H., N. Combaret, J. Dvorkin, E. Glatt, J. Han, M. Kabel, Y. Keehm, F. Krzikalla, M. Lee, C. Madonna, and M. Marsh, 2013, Digital rock physics benchmarks—Part II: Computing effective properties: Computers & Geosciences, **50**, 33-43, doi: 10.1016/j.cageo.2012.09.008.

Annan, A.P., 2005, Ground-penetrating radar: Near-surface geophysics, 357-438, doi: 10.1190/1.9781560801719.ch11.

Archie, G.E., 1942, The electrical resistivity log as an aid in determining some reservoir characteristics: Transactions of the AIME, **146**, no. 01, 54-62.

Binley, A., and L. Slater, 2020, Resistivity and Induced Polarization: Theory and Applications to the Near-Surface Earth: Cambridge University Press.

Blunt, M.J., B. Bijeljic, H. Dong, O. Gharbi, S. Iglauer, P. Mostaghimi, A. Paluszny, and C. Pentland, 2013, Pore-scale imaging and modelling: Advances in Water resources, **51**, 197-216, doi: 10.1016/j.advwatres.2012.03.003.

Bücker, M., and A. Hördt, 2013, Analytical modelling of membrane polarization with explicit parametrization of pore radii and the electrical double layer: Geophysical Journal International, **194**, no. 2, 804-813, doi: 10.1093/gji/ggt136.

Chelidze, T.L., and Y. Gueguen, 1999, Electrical spectroscopy of porous rocks: A review—I. Theoretical models: Geophysical Journal International, **137**, no. 1, 1-15, doi: 10.1046/j.1365-246x.1999.00799.x.

Chen, Y., and D. Or, 2006, Effects of Maxwell-Wagner polarization on soil complex dielectric permittivity under variable temperature and electrical conductivity: Water Resources Research, **42**, W06424 doi: 10.1029/2005WR004590.

Cheng, Y.P., M.D. Bolton, and Y. Nakata, 2004, Crushing and plastic deformation of soils simulated using DEM: Geotechnique, **54**, no. 2, 131-141, doi: 10.1680/geot.2004.54.2.131.

Choy, T.C., 2015, Effective medium theory: principles and applications (Vol. 165), Oxford University Press.

Cundall, P.A., and O.D. Strack, 1979, A discrete numerical model for granular assemblies: Geotechnique, **29**, no. 1, 47-65, doi: 10.1680/geot.1979.29.1.47.

Dvorkin, J., N. Derzhi, E. Diaz, and Q. Fang, 2011, Relevance of computational rock physics: Geophysics, **76**, no. 5, E141-E153, doi: 10.1190/geo2010-0352.1.

Feng, L., Q. Li, S.D. Cameron, K. He, R. Colby, K.M. Walker, H.W. Deckman, and D. Ertaş, 2020, Quantifying induced polarization of conductive inclusions in porous Media and implications for Geophysical Measurements: Scientific reports, **10**(1), pp.1-12.

Friedman, S.P., 2005, Soil properties influencing apparent electrical conductivity: a review: Computers and Electronics in Agriculture, **46**, no. 1-3, 45-70, doi: 10.1016/j.compag.2004.11.001.

Garboczi, E.J., 1998, Finite element and finite difference programs for computing the linear electric and elastic properties of digital images of random materials: National Institute of Standards and Technology Internal Report.

Han, T., and Y.S. Yang, 2018, Numerical and theoretical simulations of the dielectric properties of porous rocks: Journal of Applied Geophysics, **159**, 186-192, doi: 10.1016/j.jappgeo.2018.08.014.

Hanai, T., 1960, Theory of the dielectric dispersion due to the interfacial polarization and its application to emulsions: Kolloid-Zeitschrift, **171**, no. 1, 23-31.

Hanai, T., 1962, Dielectric theory on the interfacial polarization for two-phase mixtures: Bulletin of the Institute for Chemical Research, Kyoto University, **39**, no. 6.

Hauck, C., and C. Kneisel, 2006, Application of capacitively-coupled and DC electrical resistivity imaging for mountain permafrost studies: Permafrost and Periglacial Processes, **17**, no. 2, pp.169-177.

Jones, S.B., and S.P. Friedman, 2000, Particle shape effects on the effective permittivity of anisotropic or isotropic media consisting of aligned or randomly oriented ellipsoidal particles: Water Resources Research, **36**, 2821-2833, doi: 10.1029/2000WR900198.

Kemna, A., A. Binley, A. Ramirez, and W. Daily, 2000, Complex resistivity tomography for environmental applications: Chemical Engineering Journal, **77**, no. 1-2, 11-18, doi: 10.1016/S1385-8947(99)00135-7.

Kidner, N.J., B.J. Ingram, Z.J. Homrighaus, T.O. Mason, and E.J. Garboczi, 2002, Impedance/dielectric spectroscopy of electroceramics in the nanograin regime: MRS Online Proceedings Library Archive, **756**.

Kocks, U.F., C.N. Tomé, and H.R. Wenk, 2000, Texture and anisotropy: preferred orientations in polycrystals and their effect on materials properties. Cambridge university press.

Kuhn, M.R., 2006, OVAL and OVALPLOT: Programs for analyzing dense particle assemblies with the discrete element method: Department of Civil Engineering, University of Portland.

Kuras, O., D. Beamish, P.I. Meldrum, and R.D. Ogilvy, 2006, Fundamentals of the capacitive resistivity technique: Geophysics, **71**, no. 3, G135-G152, doi: 10.1190/1.2194892.

Lesmes, D.P., and F.D. Morgan, 2001, Dielectric spectroscopy of sedimentary rocks: Journal of Geophysical Research: Solid Earth, **106**, 13329-13346, doi: 10.1029/2000JB900402.

Lesmes, D. P., and S. P. Friedman, 2005, Relationships between the electrical and hydrogeological properties of rocks and soils, in Y. Rubin and S. S. Hubbard, eds., Hydrogeophysics: Springer, 87–128.

Marshall, D.J., and T.R. Madden, 1959, Induced polarization, a study of its causes: Geophysics, **24**, no. 4, 790-816, doi: 10.1190/1.1438659.

Martinez, A.L., and A.P. Barnes, 2001, Modeling dielectric-constant values of geologic materials: Midcontinent Geoscience, 1-16.

McBride, M. B., 1989, Reactions controlling heavy metal solubility in soils: Adv. Soil Sci., **10**, 1– 56, doi:10.1007/978-1-4613-8847-0_1.

Mejdoubi, A., and C. Brosseau, 2006, Finite-element simulation of the depolarization factor of arbitrarily shaped inclusions: Physical Review E, **74**, no. 3, 031405, doi: 10.1103/PhysRevE.74.031405.

Mendelson, K.S., and M.H. Cohen, 1982, The effect of grain anisotropy on the electrical properties of sedimentary rocks: Geophysics, **47**, no. 2, 257-263, doi: 10.1190/1.1441332.

Milton, G. W., D. J. Eyre, and J. V. Mantese, 1997, Finite frequency range Kramers-Kronig relations: Bounds on the dispersion: Physical Review Letters, **79**, no. 16, 3062, doi: 10.1103/PhysRevLett.79.3062.

Munoz, G., 2014, Exploring for geothermal resources with electromagnetic methods: Surveys in geophysics, **35**, no. 1, 101-122.

Niu, Q., and C. Zhang, 2017, Pore-scale modelling of complex conductivity of saturated granular materials: Near Surface Geophysics, **15**, no. 6, 593-602, doi: 10.3997/1873-0604.2017055.

Niu, Q., and C. Zhang, 2018, Physical explanation of Archie's porosity exponent in granular materials: A process-based, pore-scale numerical study: Geophysical Research Letters, **45**, 1870-1877, doi: 10.1002/2017GL076751.

Niu, Q., C. Zhang, and M. Prasad, 2020, A Framework for Pore-Scale Simulation of Effective Electrical Conductivity and Permittivity of Porous Media in the Frequency Range From 1 mHz to 1 GHz: Journal of Geophysical Research: Solid Earth, **125**, e2020JB020515, doi: 10.1029/2020JB020515.

Nobes, D.C., 1996, Troubled waters: Environmental applications of electrical and electromagnetic methods: Surveys in Geophysics, **17**, no. 4, 393-454.

Norris, A.N., A.J. Callegari, and P. Sheng, 1985, A generalized differential effective medium theory: Journal of the Mechanics and Physics of Solids, **33**, no. 6, 525-543, doi: 10.1016/0022-5096(85)90001-8.

Radjaï, F., and F. Dubois, 2011, Discrete-element modeling of granular materials: Wiley, London.

Revil, A., and P.W.J. Glover, 1998, Nature of surface electrical conductivity in natural sands, sandstones, and clays: Geophysical Research Letters, **25**, 691-694, doi: 10.1029/98GL00296.

Revil, A., 2012, S pectral induced polarization of shaly sands: Influence of the electrical double layer: Water Resources Research, **48**, W02517, doi: 10.1029/2011WR011260.

Robinson, D.A., S.B. Jones, J.M. Wraith, D. Or, and S.P. Friedman, 2003, A review of advances in dielectric and electrical conductivity measurement in soils using time domain reflectometry: Vadose Zone Journal, **2**, no. 4, 444-475.

Samouëlian, A., I. Cousin, A. Tabbagh, A. Bruand, and G. Richard, 2005, Electrical resistivity survey in soil science: a review: Soil and Tillage research, **83**, no. 2, 173-193, doi: 10.1016/j.still.2004.10.004.

Sen, P.N., C. Scala, and M.H. Cohen, 1981, A self-similar model for sedimentary rocks with application to the dielectric constant of fused glass beads: Geophysics, **46**, no. 5, 781-795, doi: 10.1190/1.1441215.

Sheng, P., and A.J. Callegari, 1984, Differential effective medium theory of sedimentary rocks: Applied Physics Letters, **44**, no. 8, 738-740, doi: 10.1063/1.94900.

Sheng, P., 1990, Effective-medium theory of sedimentary rocks: Physical Review B, **41**, no. 7, 4507, doi: 10.1103/PhysRevB.41.4507.

Simpson, F., and K. Bahr, 2005, Practical magnetotellurics: Cambridge University Press.

Sihvola, A.H., and J.A. Kong, 1988, Effective permittivity of dielectric mixtures: IEEE Transactions on Geoscience and Remote Sensing, **26**, no. 4, 420-429.

Slater, L.D., and D.R. Glaser, 2003, Controls on induced polarization in sandy unconsolidated sediments and application to aquifer characterization: Geophysics, **68**, no. 5, 1547-1558, doi: 10.1190/1.1620628.

Tabbagh, A., P. Cosenza, A. Ghorbani, R. Guérin, and N. Florsch, 2009, Modelling of Maxwell–Wagner induced polarisation amplitude for clayey materials: Journal of Applied Geophysics, **67**, no. 2, 109-113.

Topp, G.C., J.L. Davis, and A.P. Annan, 1980, Electromagnetic determination of soil water content: Measurements in coaxial transmission lines: Water resources research,**16**, 574-582, doi: 10.1029/WR016i003p00574.

Torquato, S., 2013. Random Heterogeneous Materials: Microstructure and Macroscopic Properties (Vol. 16): Springer Science & Business Media.

Torrents, J.M., T.O. Mason, and E.J. Garboczi, 2000, Impedance spectra of fiber-reinforced cement-based composites: a modeling approach: Cement and Concrete Research, **30**, no. 4, 585-592, doi: 10.1016/S0008-8846(00)00211-8.

Wagner, K.W., 1914, Electricity of the dielectric behaviour on the basis of the Maxwell theory: Arch J Elektrotech, **2**, 371-387.

Weiss, C.J., and S. Constable, 2006, Mapping thin resistors and hydrocarbons with marine EM methods, Part II—Modeling and analysis in 3D: Geophysics,**71**, no. 6, G321-G332, doi: 10.1190/1.2356908.

West, G.F., and J.C. Macnae, 1991, Physics of the electromagnetic induction exploration method, *in* Nabighian, M. N., Ed., Electromagnetic Methods in Applied Geophysics: Volume 2, Part A: Soc. Expl. Geophys., 5-45.

Wu, Y., S.S. Hubbard, C. Ulrich, and S.D. Wullschleger, 2013, Remote monitoring of freeze–thaw transitions in Arctic soils using the complex resistivity method: Vadose Zone Journal, **12**, no. 1, 1-13, doi: 10.2136/vzj2012.0062.

Zhan, X., L.M. Schwartz, M.N. Toksöz, W.C. Smith, and F.D., Morgan, 2010, Pore-scale modeling of electrical and fluid transport in Berea sandstone: Geophysics, **75**, no. 5, F135-F142, doi: 10.1190/1.3463704.

Zhao, J., and N. Guo, 2013, Unique critical state characteristics in granular media considering fabric anisotropy: Géotechnique, **63**, no. 8, 695-704, doi: 10.1680/geot.12.P.040.

Zhuravlev, L.T., 2000, The surface chemistry of amorphous silica. Zhuravlev model: Colloids and Surfaces A: Physicochemical and Engineering Aspects, **173**, no. 1-3, 1-38, doi: 10.1016/S0927-7757(00)00556-2.

Figures

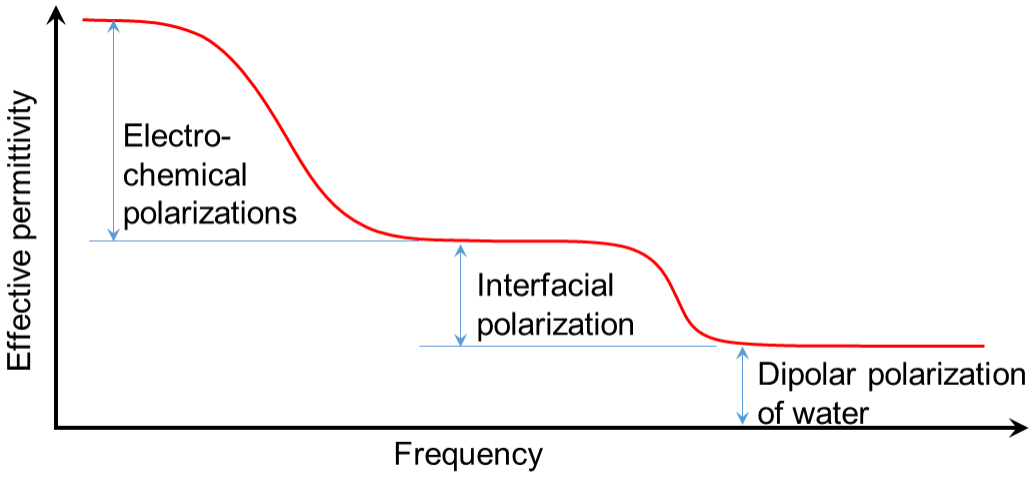

Figure 1. Frequency-dependent, effective permittivity of a typical water-saturated porous geological material.

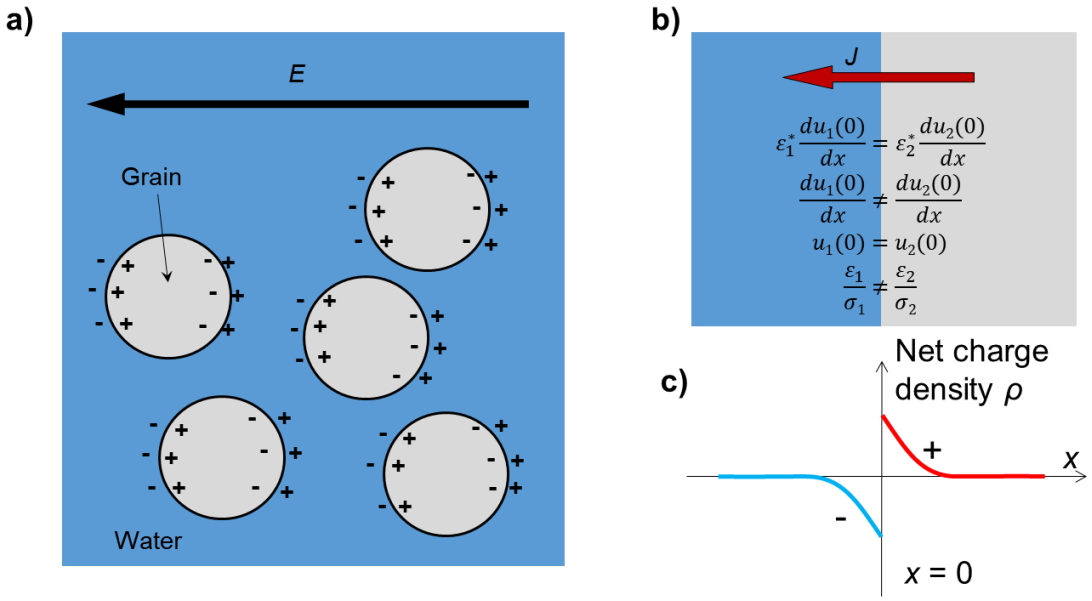

Figure 2. Interfacial polarization in a grain-water mixture: **a)** electric dipole moment at the solid-water interface induced by an external electric field, **b)** the electrical boundary conditions at the solid-water interface, and **c)** the net charge density distribution near the solid-water interface ($x = 0$).

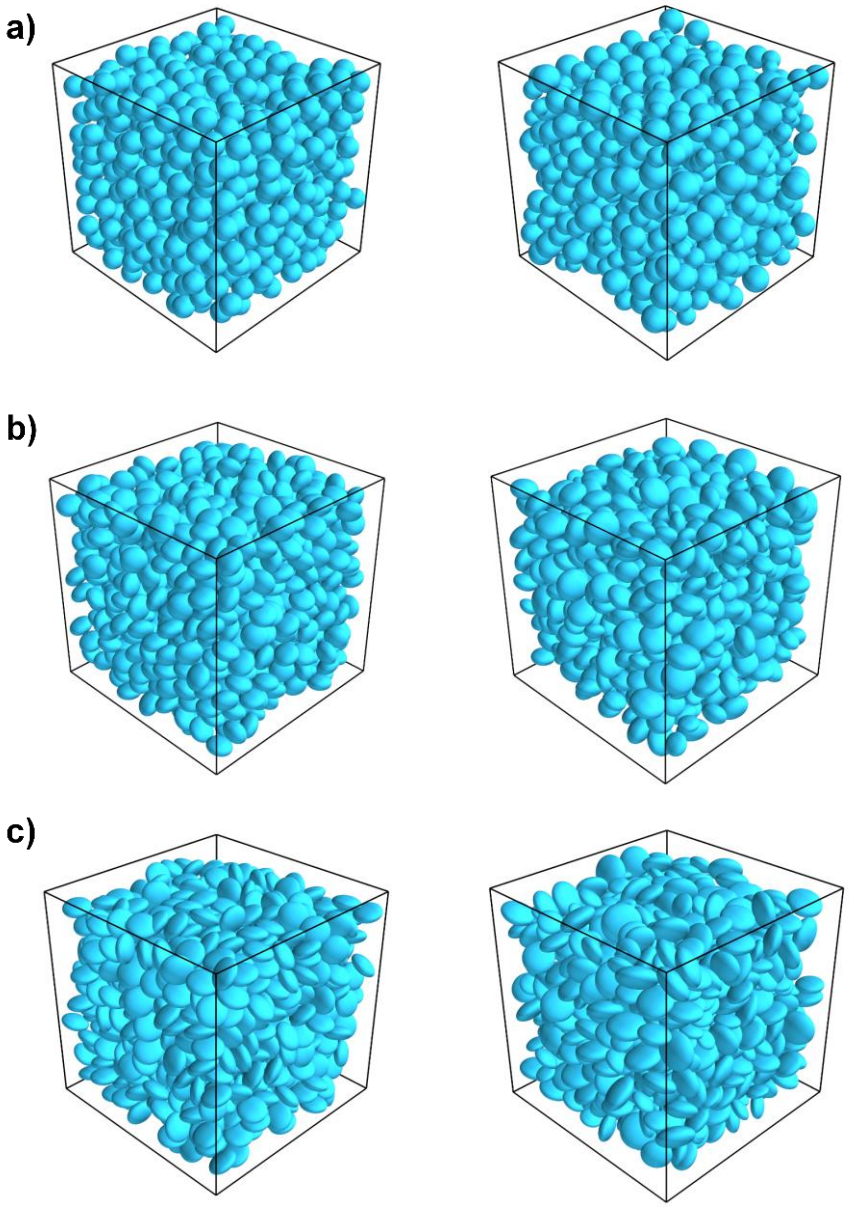

Figure 3. Synthetic granular samples used in this study: **a)** spheroidal grains with aspect ratio $e = 1$, **b)** $e = 0.67$, and **c)** $e = 0.5$. In the left panel, grains in the samples have the same size; in the right panel, grains in the samples have a distribution of sizes.

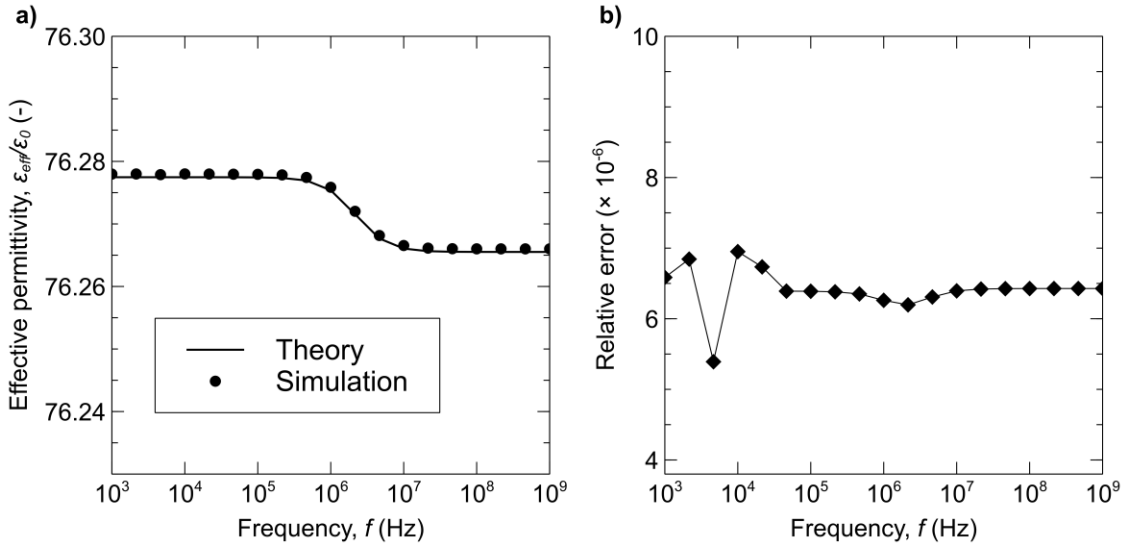

Figure 4. Benchmarking results of the numerical simulation code used in this study: **a)** theoretical and simulated effective permittivity in the frequency domain and **b)** the associated relative error (difference normalized by theoretical values). In the benchmarking, a spherical grain immersed in water is considered. The theoretical curve is obtained using equation 10, which is exact for the grain-water mixture considered here.

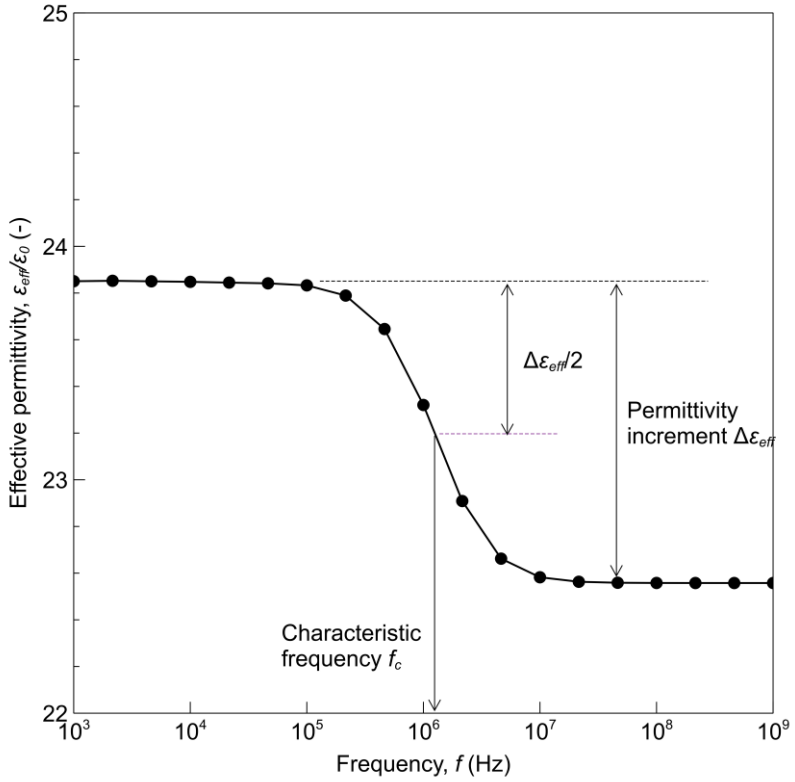

Figure 5. The definition of permittivity increment $\Delta\varepsilon_{eff}$ and characteristic frequency f_c of the interfacial polarization.

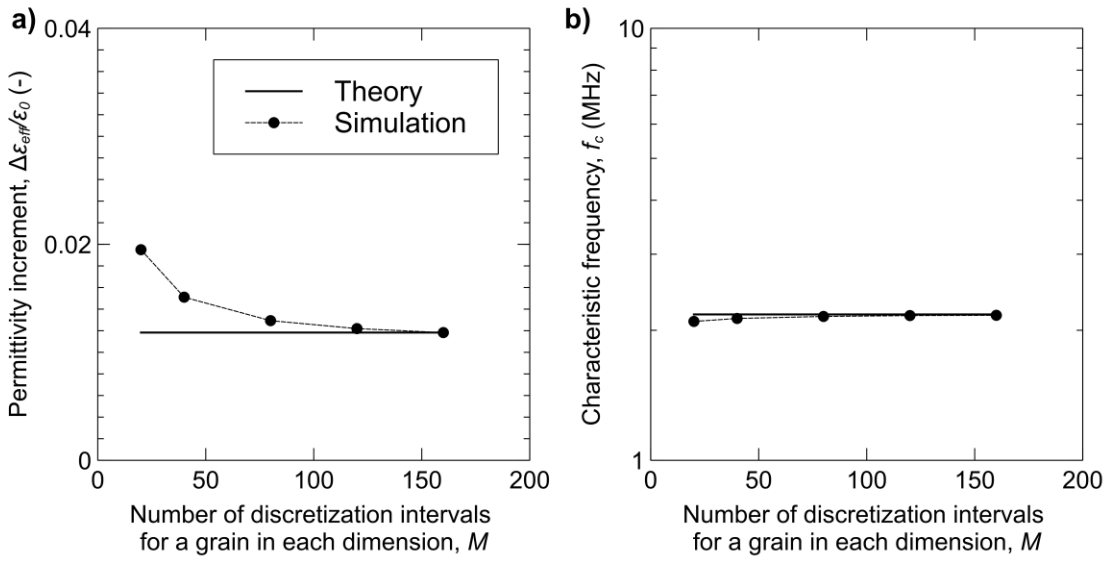

Figure 6. Influence of discretization on the calculated **a)** permittivity increment and **b)** characteristic frequency of a spherical grain immersed in water (the scale of the vertical axis is chosen to be similar to other figures in this paper for easy comparison). In our study, all the synthetic granular samples are discretized in such a way that one grain is approximately represented by ~40^3 voxels and the relative error is ~17% for permittivity increment and ~2% for the characteristic frequency.

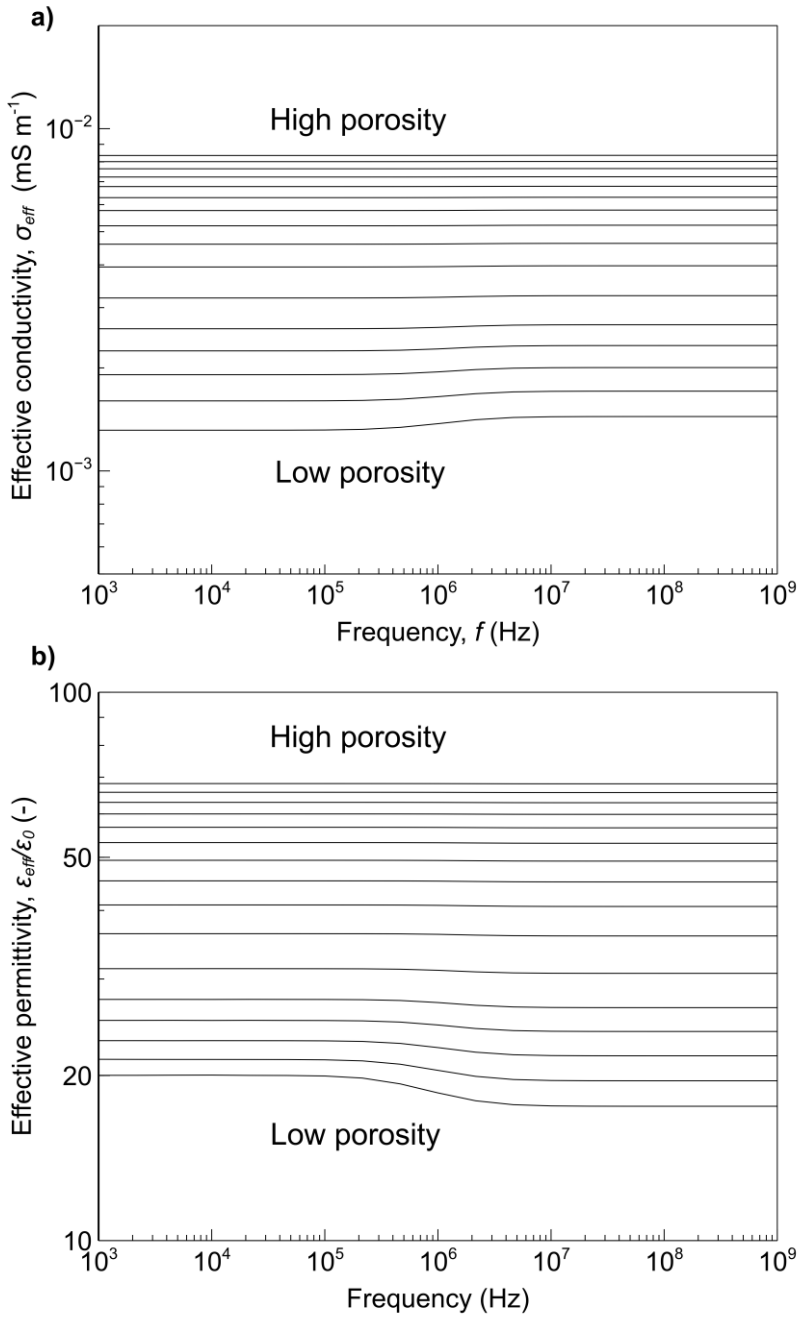

Figure 7. The frequency-dependent, effective electrical properties of a typical water-saturated granular sample (uni-sized, e = 1) with different packing density or porosity ϕ: **a)** effective conductivity and **b)** effective permittivity. In the figures, each curve corresponds to one packing density or porosity. From top to bottom, the porosity ϕ is 0.89, 0.87, 0.84, 0.81, 0.78, 0.69, 0.65, 0.60, 0.54, 0.47, 0.43, 0.40, 0.37, 0.34, and 0.30.

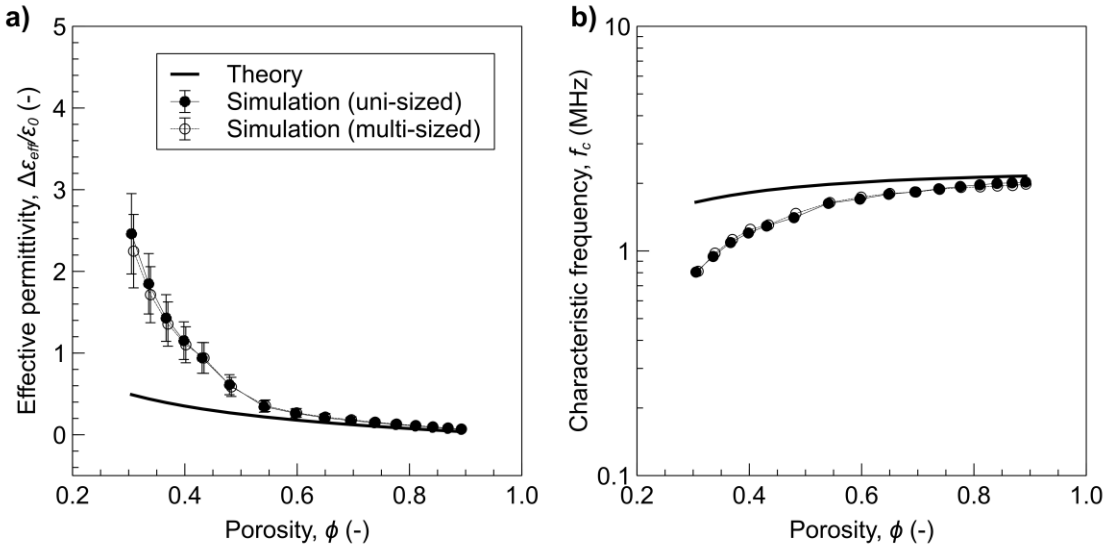

Figure 8. Effect of packing density on **a)** the permittivity increment $\Delta\varepsilon_{eff}$ and **b)** characteristic frequency f_c of interfacial polarization in the granular sample made of spheroidal grains with aspect ratio e = 1. Closed and open symbols represent the uni-sized and multi-sized samples, respectively. The solid line is the theoretical curve calculated from the DEM theory (equation 11). Error bars in **a)** represent the numerical error induced by a coarse discretization. For the characteristic frequency, the associated numerical error is smaller than the size of the symbol.

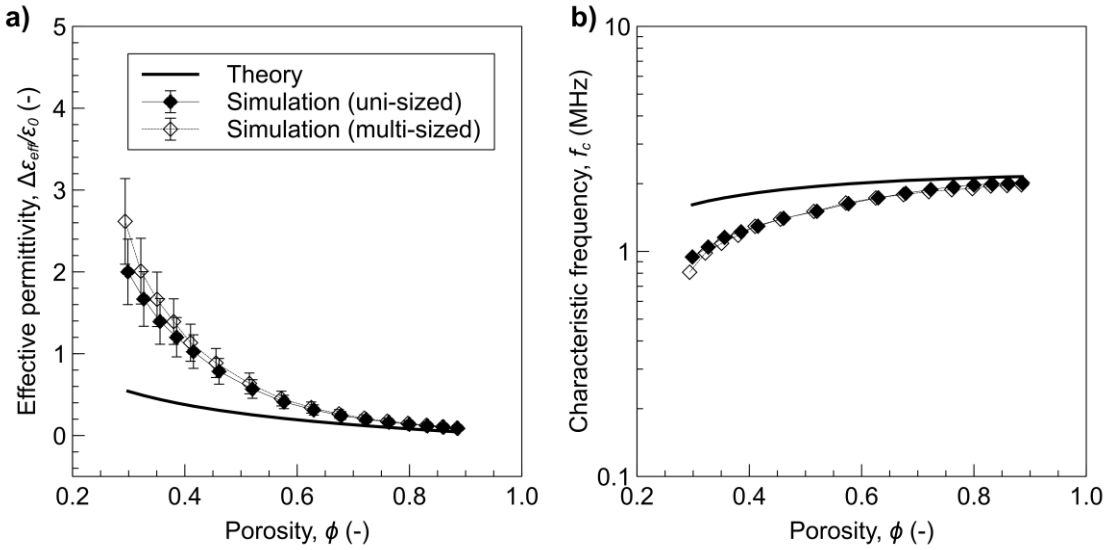

Figure 9. Effect of packing density on **a)** the permittivity increment $\Delta\varepsilon_{eff}$ and **b)** characteristic frequency f_c of interfacial polarization in the granular sample made of spheroidal grains with aspect ratio e = 0.67. Closed and open symbols represent the uni-sized and multi-sized samples, respectively. The solid line is the theoretical curve calculated from the DEM theory (equation 11). Error bars in **a)** represent the numerical error induced by a coarse discretization. For the characteristic frequency, the associated numerical error is smaller than the size of the symbol.

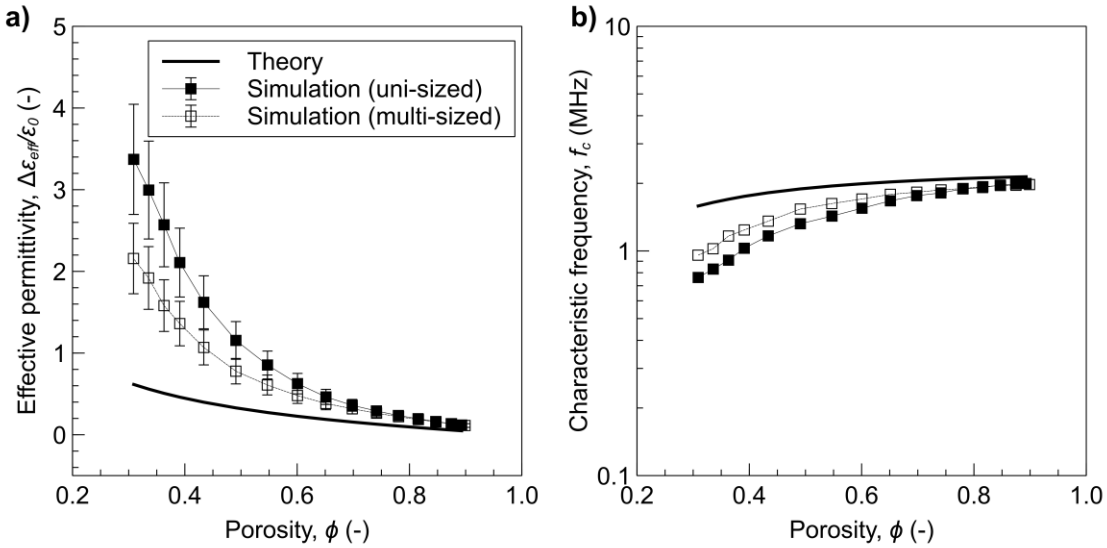

Figure 10. Effect of packing density on **a)** the permittivity increment $\Delta\varepsilon_{eff}$ and **b)** characteristic frequency f_c of interfacial polarization in the granular sample made of spheroidal grains with aspect ratio e = 0.5. Closed and open symbols represent the uni-sized and multi-sized samples, respectively. The solid line is the theoretical curve calculated from the DEM theory (equation 11). Error bars in **a)** represent the numerical error induced by a coarse discretization. For the characteristic frequency, the associated numerical error is smaller than the size of the symbol.

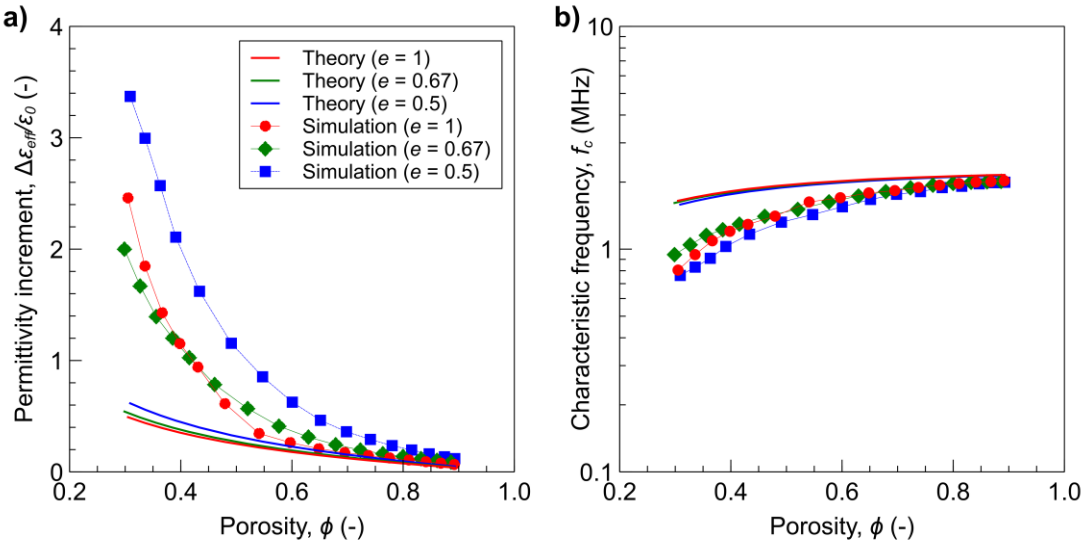

Figure 11. Effect of grain shape on **a)** the permittivity increment $\Delta\varepsilon_{eff}$ and **b)** characteristic frequency f_c of interfacial polarization in the uni-sized granular samples with different grain shapes. The theoretical results calculated from the DEM theory (equation 11) are also shown.

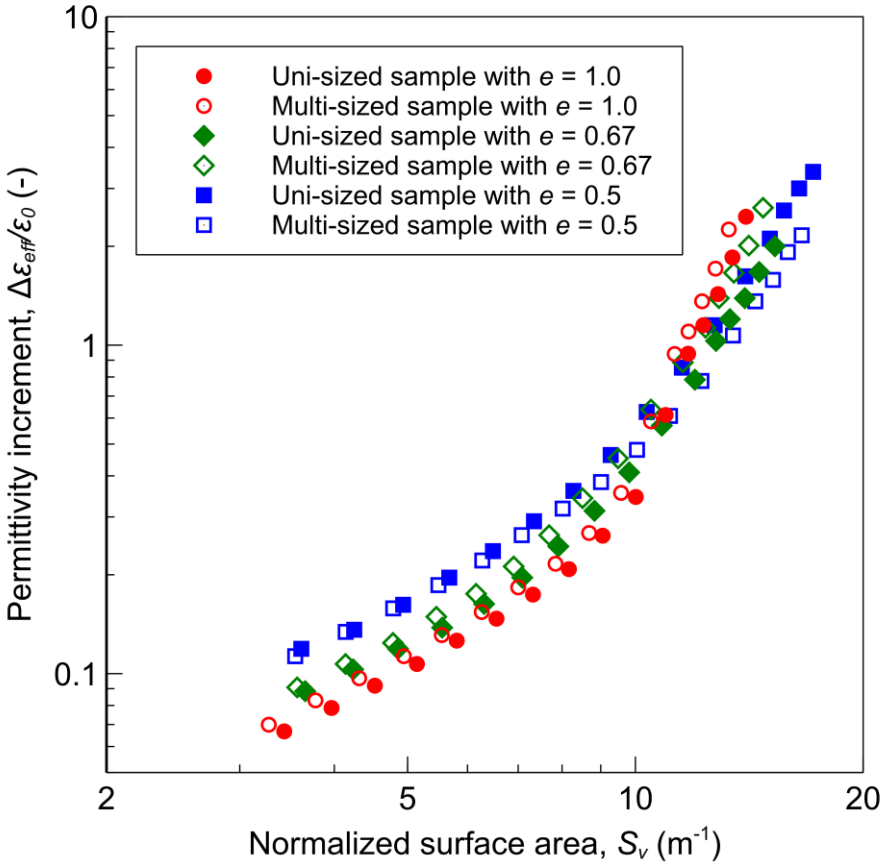

Figure 12. The correlation between permittivity increment $\Delta\varepsilon_{eff}$ and normalized surface area S_v (normalized by the sample volume) for all the six samples.

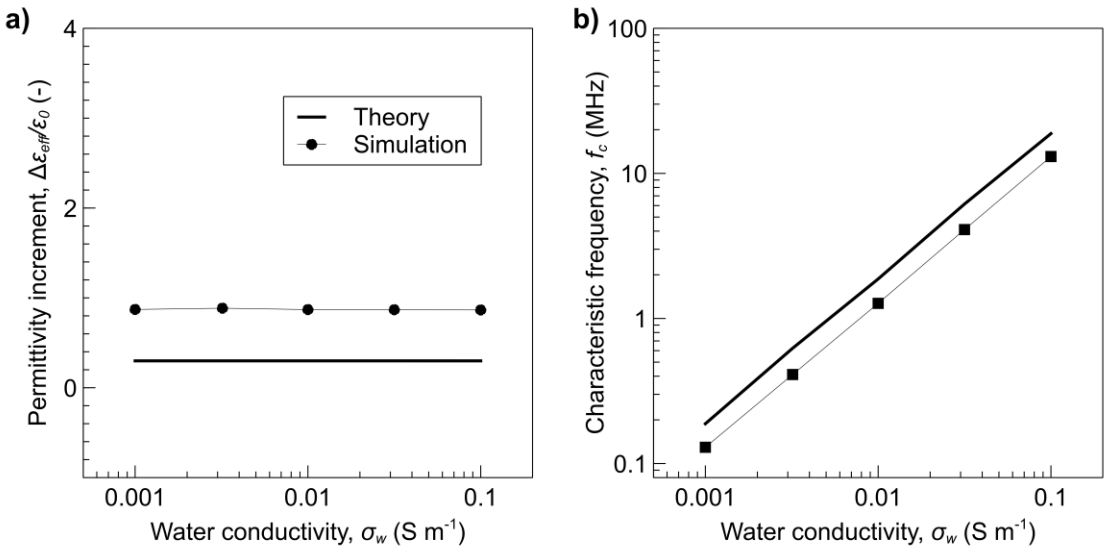

Figure 13. The effect of water conductivity σ_w on **a)** permittivity increment $\Delta\varepsilon_{eff}$ and **b)** characteristic frequency f_c of the interfacial polarization in a granular soil. Theoretical curves calculated from the DEM theory (equation 11) are also plotted for comparison. The sample is made of uni-sized spheres with a porosity of 45%.

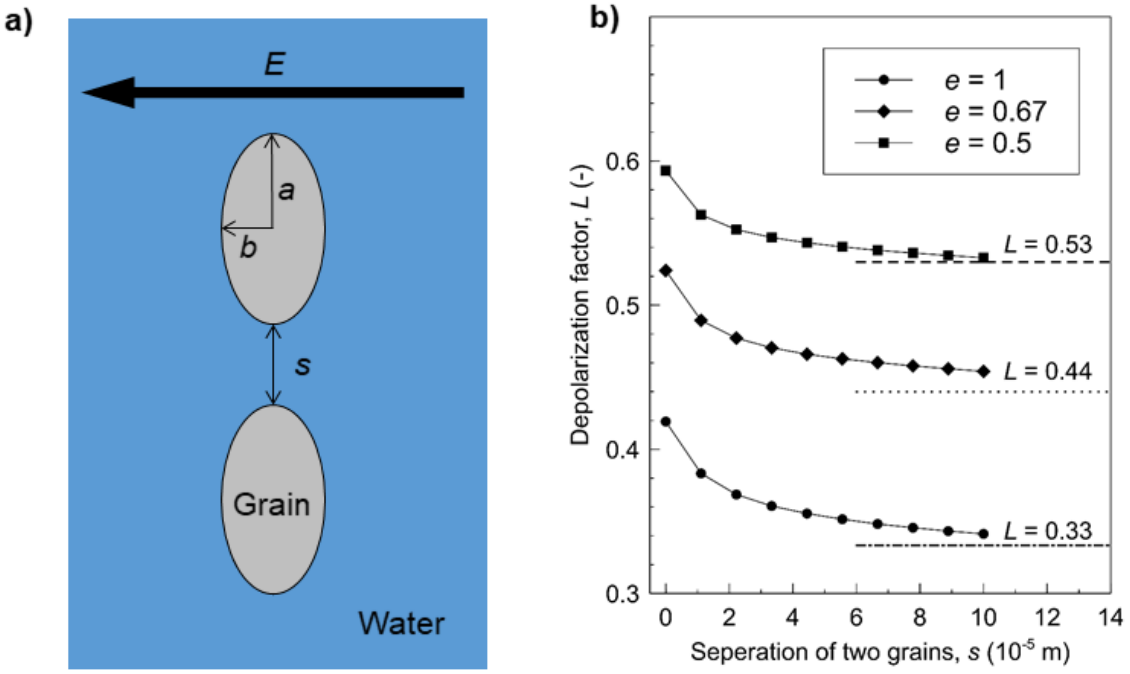

Figure 14. Electrical interactions between two neighboring spheroids: **a)** schematic showing the numerical simulation and **b)** the depolarization factor L of spheroids with different grain separations s. In the simulations, a is constant (20μm), and three grain shapes are considered. The dashed, dotted, and dash-dot lines indicate the theoretical value L = 0.53, L= 0.44, and L = 0.33 for grains with e = 0.5, 0.67, and 1, respectively.

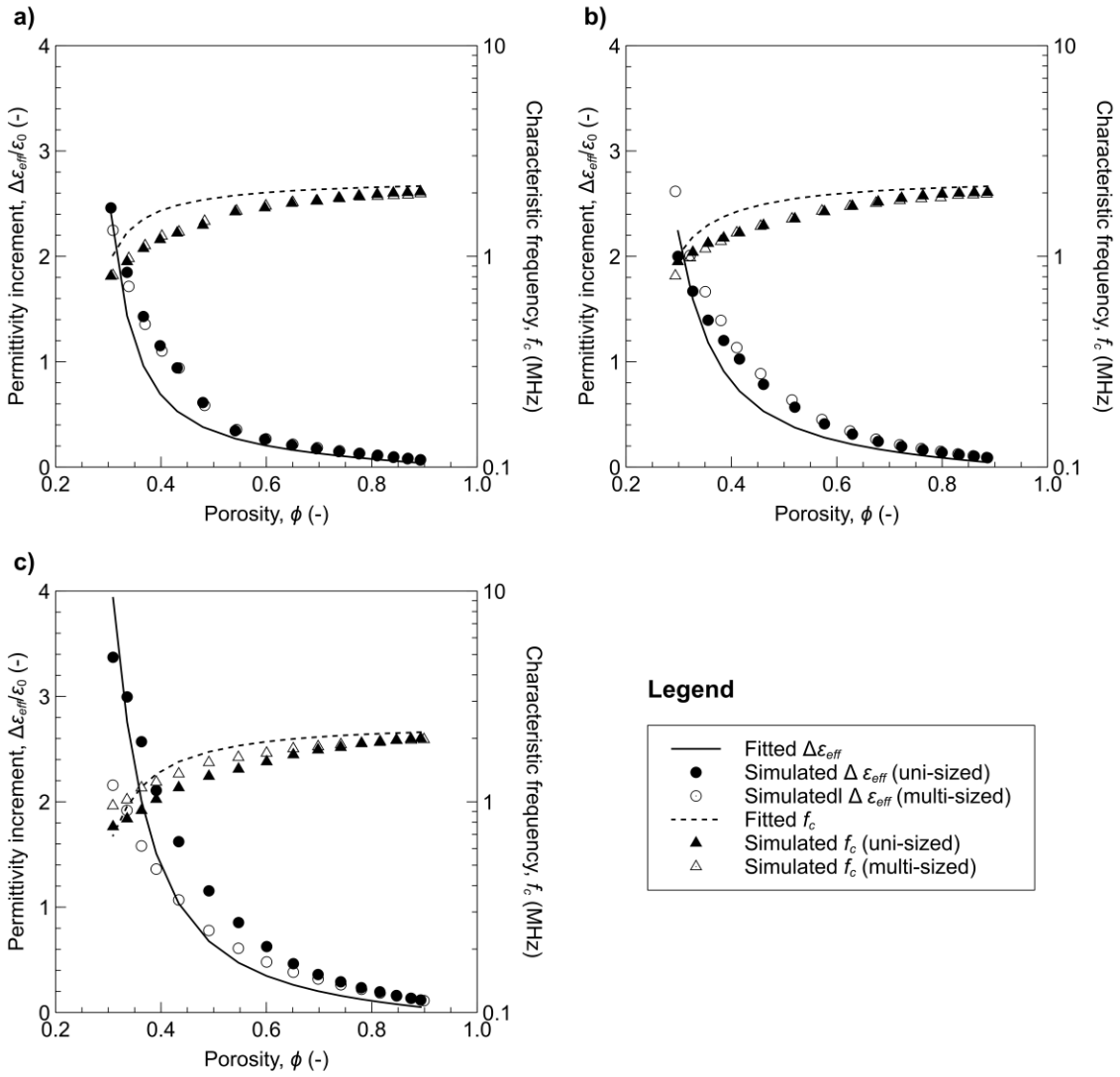

Figure 15. Fitted permittivity increment $\Delta\varepsilon_{eff}$ and characteristic frequency f_c with the existing DEM theory (equations 11 and 18) and new model for depolarization factor (equation 19): **a)** samples with e = 1, **b)** samples with e = 0.67, and **c)** samples with e = 0.5. The fitted exponent p (equation 19) is -0.72, - 0.45, and -0.38 for **a)**, **b)** and **c)**, respectively.